Zhang XH, Zhu S, Xu YL and Hong XJ (2011) Integrated optimal placement of displacement transducers and strain gauges for better estimation of structural response. *International Journal of Structural Stability and Dynamics*. 11(3): 1-22.

INTEGRATED OPTIMAL PLACEMENT OF DISPLACEMENT TRANSDUCERS AND STRAIN GAUGES FOR BETTER ESTIMATION OF STRUCTURAL RESPONSE

X. H. ZHANG[*], S. ZHU[*‡], Y. L. XU[*] and X. J. HONG[†]

[*] *Department of Civil and Structural Engineering, The Hong Kong Polytechnic University, Kowloon, Hong Kong, China*

[†] *Maunsell Structure Consulting Firm, AECOM, Shatin, N.T., Hong Kong, China*

[‡] *ceszhu@polyu.edu.hk*

Although a variety of sensors provide more comprehensive information and advanced features of structures, their distinct properties and limitations considerably complicate the design procedure of multi-type sensor systems. This paper is focused on the optimal design of integrated sensor systems with both strain gauges and displacement transducers. Unlike traditional sensor placement approaches in which these two types of sensors are often designed separately to monitor structural deformations and displacements respectively, the integrated design procedure presented in this study treats the sensor system as a whole. The number and locations of strain gauges and displacement transducers will be optimized simultaneously, and their measurement data will be fused together to better predict the unobserved structural response. The theoretical criterion for the optimization procedure is first formulated based on the strain and displacement mode shapes extracted from finite element models. Then the initial candidate sensor locations are reduced to a smaller optimal set with minimized prediction error of structural response. A two-dimensional cantilever beam is then analyzed as a numerical example to investigate the effectiveness and accuracy of the presented optimal sensor placement approach. The results indicate that the integrated sensor system provides better estimation of structural response than single-type sensor system.

Keywords: *Integrated sensor system, Sensor optimal placement, Displacement transducers, Strain gauges, noise*

1. Introduction

Structural health monitoring system (SHMS) is one of the cutting-edge technologies to assure the safety of structures during their long service lives. [1,2] Among SHMS, sensor system always plays an important role, and its spatial allocation and the quality of collected signal may affect the functionality of the entire SHMS. Considering the number of sensors is often limited, especially for those large-scale structures with great spatial complexity, the optimal sensor placement has attracted increasing interest in the past two decades. Numerous techniques have been developed for solving the optimal sensor placement problems.

To provide maximum information on the state of structures, a class of information based approaches has been extensively studied by some researchers (e.g. Ref. 3-16). In these methods, the optimal sensor locations are selected such that they maximize some norm (determinant or trace) of the Fisher information matrix (FIM) or its variants. For example, Kammer[4] proposed a method, termed Effective Independence (EfI) method, to optimize locations of vibration sensors (displacement, velocity or acceleration sensors) based on the contribution of each sensor location to the linear independence of the identified modes. This method was extended by Kammer[5] so that the number of sensors is determined during the course of sensor placement to maintain a desired level of signal-to-noise ratio. Moreover, Kammer and Tinker[8] proposed a EfI-based approach for optimal placement of triaxial accelerometers. Imamovic[13] developed the Effective Independence-Drive point residue (EfI-DPR) method which eliminates positions with low-energy content by multiplying the candidate sensor contribution to the EfI by corresponding DPR coefficients. Meo and Zumpano[15] estimated the mode shapes in remaining positions out of the observed modes in selected locations based on a statistics method called the most informative subset. The authors compared this method with other five methods, concluding that the EfI-DPR method provides an effective method for optimal sensor placement to identify the low frequency vibration characteristics. Paradinitriou *et al*.,[16] Paradinitriou[17,18] and Yuen *et al*.[19] introduced the information entropy norm to the sensor optimal placement. The optimal sensor configuration is selected as the one that minimizes the information entropy measure.

Hemez and Farhat [20] introduced another optimal sensor placement method to detect the structural damage based on strain energy distribution. Salama *et al*.[21], Chung and Moore[22], and Heo *et al*.[23] utilized the modal kinetic energy to select the optimal sensor configuration. Salama *et al*.[21] used the modal kinetic energy as a means of ranking the importance of candidate sensor locations. Heo *et al*.[23] discussed the sensor placement

optimization technique based on the maximization of the modal kinetic energy for the structural health monitoring. Its objective is to find a reduced sensor configuration which maximizes the measure of the kinetic energy of a structure. The inherent mathematical connection between the EfI and kinetic energy methods was revealed by Li *et al*.[24] Further examples of energy based sensor placement method include the eigenvalue vector product[25] and non-optimal drive point[13] methods.

Tongpadungrod *et al*.[26] used eigenvalues derived from principal component analysis as performance evaluators, and proposed an optimization technique for sensor placement. Lim[27] employed the generalized Hankel matrix, a function of the system controllability and observability, to develop a sensor placement approach to achieve a given rank of the system observability matrix while satisfying modal test constraints. Another method called modal assurance criterion (MAC) based method was presented by Carne and Dohrmann[28] to attain the sensor configuration by minimizing the off-diagonal terms in the MAC matrix. Beal *et al*.[29] formulated optimal sensor placement as a mixed variable programming (MVP) problem.

The recent development in the field of optimization algorithm has also been taken advantage of by numerous optimal sensor placement methods, such as genetic algorithms (GAs) [26,30-35] and particle swarm intelligence (PSO) [36]. Yao *et al*[30] proposed the GA as an alternative to the EfI method, choosing the determinant of the FIM as the fitness function. Worden and Burrows[31] used artificial neural network (ANN) to locate and classify faults and GA was applied to determine an optimal sensor distribution. The NN was training using mode shape curvatures. Said and Staszewski[32] utilized the GA to select the optimal sensor locations based upon the concept of mutual information. The concept was used to eliminate redundancies in information between selected sensors and rank them based on their remaining information content. Rao and Anandakumar[36] employed the PSO technique to optimize the sensor locations so as to achieve the best identification of modal frequencies and mode shapes. Many other sensor placement approaches exist in the literature, and a review is provided by Barthorpe and Worden.[37]

Nevertheless, little research has focused on the design of sensor system with multiple types of sensors. With the fast advance of sensor technology within the past two decades, the sensor network becomes more complex in terms of the number and types of sensors (e.g. strain gages, accelerometers, displacement transducers, wireless sensors, fiber optic sensors, etc). Although the variety of sensors provides more comprehensive information and advanced features, their distinct properties and limitations considerably complicate the design procedure of such hybrid sensor systems.

Therefore, this paper presents an integrated design approach of sensor systems with both strain gauges and displacement transducers. These two common types of sensors are often used to measure structural deformations and displacements separately. As a result, their spatial configurations are usually designed in two separate and distinct processes in conventional placement methodology. In view of this, this study attempts to design a sensor system including strain gauges and displacement transducers as a whole, and furthermore, the limited measurements by strain gauges and displacement transducers are fused together to estimate the response of entire structures. The integrated approach for optimal sensor placement of hybrid sensor systems is an extension of the EfI method for single-type sensor systems. The locations of strain gauges and displacement transducers are optimized simultaneously so that we can best estimate structural response of interest from limited measurements, while their total number are determined in the optimization in order to reduce estimation errors to a desired level. In particular, the normalization using noise variance is adopted to solve the problem caused by combining displacement measurements and strain measurements together. A case study of a cantilever beam is presented as an example. The results of the numerical analysis indicate that the integrated sensor system, composed of strain gauges and displacement transducers, can provide better estimation of the entire structure response than single-type sensor system.

2. Strain-Displacement Relationship

In order to integrate the design of sensor system with both strain gauges and displacement transducers, the strain-displacement relationship is first presented in this section in the context of finite element model (FEM). It is noteworthy that the strain refers to normal strains in this study since strain gauges measure only normal strains in a certain direction. The strain in an element, namely element i, can be expressed as

$$\varepsilon_i = \mathbf{B}_i \mathbf{T}_i \mathbf{S}_i \mathbf{d}_\mathbf{t} \tag{1}$$

where subscript **t** indicates that the vector corresponds to the complete set of DOFs, and thus $\mathbf{d}_\mathbf{t}$ is the displacement vector that includes translations or rotations in all degrees-of-freedom (DOFs) of a structure; **S** is a selection matrix that selects the displacements related to element i, and the number of selected DOFs is dependent on the element type; **T** is a transformation matrix that transform the element nodal displacements in global coordinates to those in local coordinate for element i; **B** is a matrix representing the relationship between the node displacements of an element and the strains in this element, which can be developed using the shape function of the element; ε_i is the strain at

a location in element *i*. Considering the strain at all the locations of interest in a structure, a strain vector can be obtained,

$$\boldsymbol{\varepsilon}_{\mathbf{t}} = (\varepsilon_1, \cdots, \varepsilon_i, \cdots, \varepsilon_n)^T = \mathbf{C}\mathbf{d}_{\mathbf{t}} \tag{2}$$

where **C** is transformation matrix between the displacement vector and the strain vector, $\mathbf{C} = ((\mathbf{B}_1\mathbf{T}_1\mathbf{S}_1)^T, (\mathbf{B}_2\mathbf{T}_2\mathbf{S}_2)^T, \cdots, (\mathbf{B}_n\mathbf{T}_n\mathbf{S}_n)^T)^T$.

In practice, reduced-order mode superposition analysis is widely adopted to calculate the dynamic response of linear systems with a large number of DOFs. A modal expansion of the displacement vector yields

$$\mathbf{d}_{\mathbf{t}} \approx \sum_{r=1}^{k} \phi_r q_r = \boldsymbol{\Phi}_{\mathbf{t}}\mathbf{q} \tag{3}$$

where $\boldsymbol{\Phi}_{\mathbf{t}}$ is the displacement modal matrix consisting of mass normalized displacement modes shapes ϕ_r that can be obtained by modal analysis of finite element model; **q** is the modal coordinates; the number of mode shapes *k* considered is usually much less than the total number of DOFs for large-scale structures. In general, $\boldsymbol{\Phi}_{\mathbf{t}}$ should include all important mode shapes excited by external loads, and the value of *k* should be determined in consideration of modal contribution factors, frequency bandwidth of excitations and sampling rate of data acquisition.

Subsequently, the strain vector can be expressed with the modal coordinates:

$$\boldsymbol{\varepsilon}_{\mathbf{t}} = \sum_{r=1}^{k} \psi_r q_r = \boldsymbol{\Psi}_{\mathbf{t}}\mathbf{q} \tag{4}$$

$$\psi_r = \mathbf{C}\phi_r, \qquad \boldsymbol{\Psi}_{\mathbf{t}} = \mathbf{C}\boldsymbol{\Phi}_{\mathbf{t}} \tag{5}$$

where the vector ψ_r is the strain model shape corresponding to the displacement mode shape ϕ_r; and $\boldsymbol{\Psi}_{\mathbf{t}}$ is strain modal matrix.

The transformation matrices **B**, **T** and **S** are all dependent on the element type, as different types of elements have different number of nodes, local coordinate systems and shapes functions. An example is presented hereunder for the two-dimensional, prismatic and symmetric beam element which is later employed in the case study of this paper. The planar beam is a 6-DOF element, and its normal strain of a beam can be divided into the

deformations due to axial force and bending moment respectively. The displacement-strain relationship for the planar beam element can be obtained as follows[38]

$$\begin{Bmatrix} \varepsilon_x \\ \varepsilon_b \end{Bmatrix} = \begin{Bmatrix} \dfrac{du}{dx} \\ -y\dfrac{d^2v}{dx^2} \end{Bmatrix} = \begin{Bmatrix} H_u'(x) \\ -yH_v''(x) \end{Bmatrix} \mathbf{A}d_e \tag{6}$$

where d_e is the nodal displacement vector corresponding to 6 DOFs of the beam element, x and y denote the location in the element coordinate where the strain is calculated, and u and v is the shape functions which can be expressed by the functions $H_u(x)$ and $H_v(x)$ and the matrix **A**,

$$H_u = \begin{bmatrix} 1 & 0 & 0 & x & 0 & 0 \end{bmatrix} \tag{7}$$

$$H_v = \begin{bmatrix} 0 & 1 & x & 0 & x^2 & x^3 \end{bmatrix} \tag{8}$$

$$\mathbf{A} = \begin{bmatrix} 1 & 0 & 0 & 0 & 0 & 0 \\ 0 & 1 & 0 & 0 & 0 & 0 \\ 0 & 0 & 1 & 0 & 0 & 0 \\ -1/l & 0 & 0 & 1/l & 0 & 0 \\ 0 & -3/l^2 & -2/l & 0 & 3/l^2 & -1/l \\ 0 & 2/l^3 & 1/l^2 & 0 & -2/l^3 & 1/l^2 \end{bmatrix} \tag{9}$$

where l is the length of the beam element. As mentioned before, the actual normal strain is the superposition of two components, i.e. $\varepsilon=\varepsilon_x+\varepsilon_b$, and thus the strain-displacement relationship matrix for the planar beam element reads

$$\mathbf{B} = \begin{bmatrix} H_u'(x) - yH_v''(x) \end{bmatrix} \mathbf{A} \tag{10}$$

The strain-displacement relationships for other element types can be derived in a similar way, e.g. three-dimensional beam element and plate element, although they may be more complex.

3. Optimization Strategy

The number of sensor measurement is always limited in comparison with the number of structural responses of interest, especially for large-scale structures. It is necessary to estimate some quantities based on the limited measurement. Therefore, the optimal sensor placement presented in this section aims to minimize the error in the estimation of

unmeasured displacements and strains. In particular, the locations of strain gauges and displacement transducers are optimized simultaneously, unlike the conventional design methodology in which they were usually carried out in two separate and distinct processes. The estimation process also employs both the strain and displacement measurements. The total number of both sensors is determined within the optimization procedure based on the target error levels of the estimation instead of being prescribed.

Assume the response vector **y** includes the displacements and strains at the locations of interest for a structure, i.e. $\mathbf{y} = \begin{bmatrix} \boldsymbol{\varepsilon} & \mathbf{d} \end{bmatrix}^T$. For a linear structural system, the response can be expressed as a linear combination of a small subset of mode shapes[39]

$$\mathbf{y} = \begin{Bmatrix} \boldsymbol{\varepsilon} \\ \mathbf{d} \end{Bmatrix} = \begin{Bmatrix} \boldsymbol{\Psi} \\ \boldsymbol{\Phi} \end{Bmatrix} \mathbf{q} = \boldsymbol{\Gamma} \mathbf{q} \tag{11}$$

where **q** is the vector of modal coordinates; **Γ** is the general modal matrix which includes both strain mode shapes **Ψ** and displacement mode shapes **Φ**. As mentioned before, it is not practical to include all mode shapes for large-scale structures, and usually only a subset of k mode shapes corresponding to low frequencies are considered. The dimension of the response vector **y,** denoted as n, represents the total number of candidate positions, whereas the dimensions of vectors **ε** and **d**, denoted as n^{ε} and n^{d}, represent the number of candidate locations for strain gauges and displacement transducers respectively. Therefore, the sizes of the matrices **Γ**, **Ψ** and **Φ** are $n \times k$, $n^{\varepsilon} \times k$ and $n^{\mathrm{d}} \times k$ respectively. Note that n is much less than total number of DOFs as only displacements and strains of interest are considered here. Thus **Ψ** and **Φ** are only sub-matrices of aforementioned modal matrices $\boldsymbol{\Psi}_{\mathbf{t}}$ and $\boldsymbol{\Phi}_{\mathbf{t}}$.

The objective of the sensor placement strategy is to select a subset of candidate positions for the placement of strain gauges and displacement transducers. Assume the total of n_{m} locations are chosen, $n_{\mathrm{m}} = n^{\varepsilon}_{\mathrm{m}} + n^{\mathrm{d}}_{\mathrm{m}}$, where the subscript m denotes the measurement, and $n^{\varepsilon}_{\mathrm{m}}$ and $n^{\mathrm{d}}_{\mathrm{m}}$ denote the number of strain gauges and displacement transducers respectively. From Eq. (11), the measured response can be expressed as

$$\mathbf{y}_{\mathbf{m}} = \begin{Bmatrix} \boldsymbol{\Psi}_{\mathbf{m}} \\ \boldsymbol{\Phi}_{\mathbf{m}} \end{Bmatrix} \mathbf{q} + \mathbf{w} = \boldsymbol{\Gamma}_{\mathbf{m}} \mathbf{q} + \mathbf{w} \tag{12}$$

where $\boldsymbol{\Gamma}_{\mathbf{m}}$, $\boldsymbol{\Psi}_{\mathbf{m}}$ and $\boldsymbol{\Phi}_{\mathbf{m}}$ are partitioned model matrices corresponding to the positions with sensors, and **w** represents the noise vector in the measurement. Note that the dimension of $\boldsymbol{\Gamma}_{\mathbf{m}}$ is much smaller than total DOFs of structures. For example, rotational DOFs are often not included as it is difficult to measure the corresponding response. In addition, the strain

mode shapes are also added into $\mathbf{\Gamma_m}$, and $\mathbf{\Gamma_m}$ is no longer orthogonal to stiffness and mass matrix. Therefore the modal coordinates could not be solved via modal orthogonality properties. O'Callahan[40] introduced the System Equivalent Reduction-Expansion Process (SEREP) method to estimate the response at unmeasured DOFs based on the limited measurement. In this method the pseudo-verse of modal matrix is used to get the least square solutions for modal coordinates. Similar approach is adopted here to estimate the response vector $\mathbf{y}$,

$$\mathbf{y_e} = \mathbf{\Gamma}\ \mathbf{\Gamma_m^+}\ \mathbf{y_m} \tag{13}$$

where the subscript e denotes the estimation. However, the estimated response vector $\mathbf{y_e}$ herein includes the displacement response and strain response, both measured and unmeasured. $\mathbf{\Gamma_m^+}$ denotes the pseudo-inverse of the matrix $\mathbf{\Gamma_m}$, and it can be calculated by $\mathbf{\Gamma_m^+} = (\mathbf{\Gamma_m^T \Gamma_m})^{-1}\mathbf{\Gamma_m^T}$ provided that $\mathbf{\Gamma_m}$ is of full column rank. It should be noted that the strain response and the displacement response have different order of magnitude, and thus the matrix $\mathbf{\Gamma_m}$ may be ill conditioned. Using Eq. (13) directly to estimate structural response is not usually practical especially for large-scale structures.

Kammer[4] proposed the Effective Independence (EfI) method for the optimal placement of displacement, velocity or acceleration sensors based on the contribution of each sensor location to the linear independence of the identified modes. Later Kammer[5] extended the EfI method to include the effects of measurement noise, where the number of sensors is determined based on a predetermined level of signal-to-noise ratio in modal coordinates. This approach is further extended to achieve the optimal placement of sensor system with both displacement transducers and strain gauges. The estimation error of response vector $\mathbf{y_e}$ is first quantified, and the total number of displacement transducers and strain gauges and their optimal locations are both determined in an optimization procedure with the objective of minimizing the estimation error.

The error between the estimated response and the real response, $\mathbf{\Delta}$, can be obtained from Eqs. (11), (12) and (13):

$$\mathbf{\delta} = \mathbf{y_e} - \mathbf{y} = \mathbf{\Gamma q} + \mathbf{\Gamma\Gamma_m^+ w} - \mathbf{\Gamma q} = \mathbf{\Gamma\Gamma_m^+ w} \tag{14}$$

Subsequently the covariance matrix of the estimation error can be calculated as

$$\mathbf{\Delta} = E(\mathbf{\delta\delta^T}) = E[\mathbf{\Gamma\Gamma_m^+ w w^T (\Gamma_m^+)^T \Gamma^T}] = \mathbf{\Gamma\Gamma_m^+} E(\mathbf{w w^T})\mathbf{(\Gamma_m^+)^T \Gamma^T} \tag{15}$$

where $E(\cdot)$ is the expected value operator, and $E(\mathbf{w}\mathbf{w}^{\mathrm{T}})$ is the covariance matrix of the measurement noise. The measurement noise is often assumed as a zero-mean stationary Gaussian noise. It is assumed in this study that the sensor noise is uncorrelated with each other, and each type of sensors is of equal variance, and this yields [41]

$$E(\mathbf{w}\mathbf{w}^{\mathbf{T}}) = \begin{bmatrix} \sigma_{\varepsilon}^2\mathbf{I} & \\ & \sigma_d^2\mathbf{I} \end{bmatrix} = \boldsymbol{\Sigma}_{\mathbf{m}}^{\mathbf{2}} \tag{16}$$

where σ_{ε}^2 is the strain gauges noise variance, σ_d^2 is the displacement transducers noise variance, $\mathbf{I}$ denotes the identity matrix, and matrix $\boldsymbol{\Sigma}$ is a diagonal matrix that reads

$$\boldsymbol{\Sigma} = \begin{bmatrix} \sigma_{\varepsilon}\mathbf{I} & \\ & \sigma_d\mathbf{I} \end{bmatrix} \tag{17}$$

The subscript m indicates that the dimension of the matrix $\boldsymbol{\Sigma}_{\mathbf{m}}$ is equal to the total number of measurement locations. Eq. (15) can be rewritten as

$$\boldsymbol{\Delta} = E(\boldsymbol{\delta}\boldsymbol{\delta}^{\mathbf{T}}) = \boldsymbol{\Gamma}\boldsymbol{\Gamma}_{\mathbf{m}}^{+}\boldsymbol{\Sigma}_{\mathbf{m}}^{\mathbf{2}}(\boldsymbol{\Gamma}_{\mathbf{m}}^{+})^{\mathbf{T}}\boldsymbol{\Gamma}^{\mathbf{T}} = (\boldsymbol{\Gamma}\boldsymbol{\Gamma}_{\mathbf{m}}^{+}\boldsymbol{\Sigma}_{\mathbf{m}})(\boldsymbol{\Gamma}\boldsymbol{\Gamma}_{\mathbf{m}}^{+}\boldsymbol{\Sigma}_{\mathbf{m}})^{T} \tag{18}$$

$\boldsymbol{\Delta}$ is the covariance matrix of the estimation error, and each diagonal element represents the variance of the estimation error for corresponding response (strain or displacement). Therefore, the maximum diagonal element denotes the maximum estimation error, while the trace of the matrix $\boldsymbol{\Delta}$ represents the sum of estimation errors at all locations of interest. Consequently, the sensors optimal placement can be done by minimizing the maximum estimation error, total estimation error or both.

As mentioned before, however, the magnitudes of strain and displacement responses are of different orders, and as such their absolute estimation errors. The optimization procedure may considerably bias one type of sensors. In view of this, the relative estimation error-the ratio of the estimation error to the measurement noise-is used in this study

$$\widetilde{\boldsymbol{\delta}} = \begin{Bmatrix} \dfrac{\boldsymbol{\varepsilon}_{\mathbf{e}} - \boldsymbol{\varepsilon}}{\sigma_{\varepsilon}} \\ \dfrac{\mathbf{d}_{\mathbf{e}} - \mathbf{d}}{\sigma_d} \end{Bmatrix} = \boldsymbol{\Sigma}^{-\mathbf{1}}\boldsymbol{\delta} \tag{19}$$

Similarly, the noise-normalized mode shape matrices are defined as $\widetilde{\boldsymbol{\Psi}} = \dfrac{1}{\sigma_{\varepsilon}} \cdot \boldsymbol{\Psi}$,

$\widetilde{\mathbf{\Phi}} = \frac{1}{\sigma_d} \cdot \mathbf{\Phi}$, $\widetilde{\mathbf{\Psi}}_\mathbf{m} = \frac{1}{\sigma_\varepsilon} \cdot \mathbf{\Psi}_\mathbf{m}$, $\widetilde{\mathbf{\Phi}}_\mathbf{m} = \frac{1}{\sigma_d} \cdot \mathbf{\Phi}_\mathbf{m}$. Thus

$$\widetilde{\mathbf{\Gamma}} = \begin{bmatrix} \widetilde{\mathbf{\Psi}} & \widetilde{\mathbf{\Phi}} \end{bmatrix}^\mathbf{T} = \mathbf{\Sigma}^{-1}\mathbf{\Gamma} \tag{20}$$

$$\widetilde{\mathbf{\Gamma}}_\mathbf{m} = \begin{bmatrix} \widetilde{\mathbf{\Psi}}_\mathbf{m} & \widetilde{\mathbf{\Phi}}_\mathbf{m} \end{bmatrix}^\mathbf{T} = \mathbf{\Sigma}_\mathbf{m}^{-1}\mathbf{\Gamma}_\mathbf{m} \tag{21}$$

and the noise-normalized response vectors

$$\widetilde{\mathbf{y}} = \mathbf{\Sigma}^{-1} \cdot \mathbf{y} = \widetilde{\mathbf{\Gamma}}\mathbf{q} \tag{22}$$

$$\widetilde{\mathbf{y}}_\mathbf{m} = \mathbf{\Sigma}_m^{-1} \cdot \mathbf{y}_\mathbf{m} = \widetilde{\mathbf{\Gamma}}_\mathbf{m}\mathbf{q} + \mathbf{\Sigma}_\mathbf{m}^{-1}\mathbf{w} \tag{23}$$

where '~' denotes the noise-normalized vectors or matrices. Note that the matrices $\mathbf{\Sigma_m}$ and $\mathbf{\Sigma}$ have different dimensions despite the similar format. The estimation of the structural response can be computed by

$$\widetilde{\mathbf{y}}_\mathbf{e} = \widetilde{\mathbf{\Gamma}}\,\widetilde{\mathbf{\Gamma}}_\mathbf{m}^{+}\,\widetilde{\mathbf{y}}_\mathbf{m} \tag{24}$$

$$\mathbf{y}_\mathbf{e} = \mathbf{\Sigma}\,\widetilde{\mathbf{\Gamma}}\,\widetilde{\mathbf{\Gamma}}_\mathbf{m}^{+}\,\widetilde{\mathbf{y}}_\mathbf{m} = \mathbf{\Gamma}\,\widetilde{\mathbf{\Gamma}}_\mathbf{m}^{+}\,\widetilde{\mathbf{y}}_\mathbf{m} \tag{25}$$

Note that the noise-normalized modal matrix $\widetilde{\mathbf{\Gamma}}_\mathbf{m}$ has much lower condition number, and considerably improves the accuracy of the calculation especially for large-scale structures. The covariance matrix of the normalized estimation error vector can be computed as

$$\begin{aligned} \widetilde{\mathbf{\Lambda}} = E(\widetilde{\boldsymbol{\delta}}\widetilde{\boldsymbol{\delta}}^\mathbf{T}) &= \widetilde{\mathbf{\Gamma}}\widetilde{\mathbf{\Gamma}}_\mathbf{m}^{+}\mathbf{\Sigma}_\mathbf{m}^{-1}E(\mathbf{w}\mathbf{w}^\mathbf{T})(\mathbf{\Sigma}_\mathbf{m}^{-1})^\mathbf{T}(\widetilde{\mathbf{\Gamma}}_\mathbf{m}^{+})^\mathbf{T}\widetilde{\mathbf{\Gamma}}^\mathbf{T} = \widetilde{\mathbf{\Gamma}}\widetilde{\mathbf{\Gamma}}_\mathbf{m}^{+}(\widetilde{\mathbf{\Gamma}}_\mathbf{m}^{+})^\mathbf{T}\widetilde{\mathbf{\Gamma}}^\mathbf{T} \\ &= \widetilde{\mathbf{\Gamma}}(\widetilde{\mathbf{\Gamma}}_\mathbf{m}^\mathbf{T}\widetilde{\mathbf{\Gamma}}_\mathbf{m})^{-1}(\widetilde{\mathbf{\Gamma}}_\mathbf{m}^\mathbf{T}\widetilde{\mathbf{\Gamma}}_\mathbf{m})(\widetilde{\mathbf{\Gamma}}_\mathbf{m}^\mathbf{T}\widetilde{\mathbf{\Gamma}}_\mathbf{m})^{-1}\widetilde{\mathbf{\Gamma}}^\mathbf{T} \\ &= \widetilde{\mathbf{\Gamma}}(\widetilde{\mathbf{\Gamma}}_\mathbf{m}^\mathbf{T}\widetilde{\mathbf{\Gamma}}_\mathbf{m})^{-1}\widetilde{\mathbf{\Gamma}}^\mathbf{T} \end{aligned} \tag{26}$$

The diagonal elements of the matrix $\widetilde{\mathbf{\Lambda}}$ represent the variances of normalized estimation error

$$diag(\widetilde{\mathbf{\Lambda}}) = \begin{bmatrix} \widetilde{\sigma}_1^2 & \widetilde{\sigma}_2^2 & \cdots & \widetilde{\sigma}_n^2 \end{bmatrix} \tag{27}$$

and they are of the same order of magnitude for displacement transducers and strain gauges. Therefore, such normalization enables the simultaneous selection of the optimal locations

of displacement transducers and strain gauges. A weight matrix **P** can be applied to account for the importance of different locations, or the different requirement on the normalized estimation error for strain gauges and displacement transducers.

$$\widetilde{\mathbf{\Delta}}_{\mathrm{w}} = \mathbf{P}\widetilde{\mathbf{\Delta}}, \qquad diag(\widetilde{\mathbf{\Delta}}_{\mathrm{w}}) = \begin{bmatrix} p_1\widetilde{\sigma}_1^2 & p_2\widetilde{\sigma}_2^2 & \cdots & p_n\widetilde{\sigma}_n^2 \end{bmatrix}$$

The maximum and average estimation errors at all locations can be computed by

$$\begin{aligned} \widetilde{\sigma}_{\max}^2 &= \max(diag(\widetilde{\mathbf{\Delta}}_{\mathrm{w}})) \\ \widetilde{\sigma}_{avg}^2 &= \frac{tr(\widetilde{\Delta}_{\mathrm{w}})}{n} = \frac{tr\left[\mathbf{P}\widetilde{\mathbf{\Gamma}}(\widetilde{\mathbf{\Gamma}}_{\mathbf{m}}^{\mathrm{T}}\widetilde{\mathbf{\Gamma}}_{\mathbf{m}})^{-1}\widetilde{\mathbf{\Gamma}}^{\mathrm{T}}\right]}{n} = \frac{tr\left[\mathbf{P}(\widetilde{\mathbf{\Gamma}}^{\mathrm{T}}\widetilde{\mathbf{\Gamma}})(\widetilde{\mathbf{\Gamma}}_{\mathbf{m}}^{\mathrm{T}}\widetilde{\mathbf{\Gamma}}_{\mathbf{m}})^{-1}\right]}{n} \end{aligned} \tag{28}$$

where $tr(\cdot)$ denotes the trace of the enclosed matrix. In this study, the weight matrix is taken as an identity matrix, and the optimization objective in this study is

$$\text{minimize } \widetilde{\sigma}_{avg}^2 \Rightarrow \text{minimize } tr\left[(\widetilde{\mathbf{\Gamma}}^{\mathrm{T}}\widetilde{\mathbf{\Gamma}})(\widetilde{\mathbf{\Gamma}}_{\mathbf{m}}^{\mathrm{T}}\widetilde{\mathbf{\Gamma}}_{\mathbf{m}})^{-1}\right] \tag{29}$$

subject to

$$\widetilde{\sigma}_{\max}^2 \le [\widetilde{\sigma}_{\max}^2] \ , \quad \widetilde{\sigma}_{avg}^2 \le [\widetilde{\sigma}_{avg}^2] \tag{30}$$

in which $[\widetilde{\sigma}_{\max}^2]$ and $[\widetilde{\sigma}_{avg}^2]$ are the target normalized maximum and average estimated errors respectively.

The maximum and average estimation errors will be increased with the reduction of the number of sensors. The total number of strain gauges and displacement transducers can be thus determined to achieve the prescribed criterion for estimation errors, as shown in constraint functions. A simple iterative procedure is carried out, in which the candidate sensor positions are deleted one by one until the target error level is reached. In each step, one sensor location is removed which results in a minimal trace of the matrix $(\widetilde{\mathbf{\Gamma}}^{\mathrm{T}}\widetilde{\mathbf{\Gamma}})(\widetilde{\mathbf{\Gamma}}_{\mathbf{m}}^{\mathrm{T}}\widetilde{\mathbf{\Gamma}}_{\mathbf{m}})^{-1}$. Once the sensor locations are identified, the response at other locations can be estimated using Eq. (25). It should be noted that such a simple procedure can be only applied to relative simple structures. For large-scale or complex structures with a large number of DOFs, this procedure is time-consuming and possibly suboptimal. Some common optimization methods, e.g. genetic algorithm, could be employed in that case.

4. Case Study

A cantilever beam with a length of about 2.0 m and a cross section of 50.8mm×50.8mm is employed in the analytical study. The beam is modeled by two-dimensional beam element described before, and the finite-element model consists of 21 nodes and 20 equal-length elements ((as shown in Fig. 1(a)). A random excitation is applied vertically at the end of the cantilever beam, and it induces the flexural vibration of the beam. It should be pointed out that the proposed approach is not dependent on the input excitation, and any other types of excitation (e.g. harmonic load) can be applied as well. It may be considered as a merit of this approach, as the input excitation is often hardly measured in real structures. The random force is adopted only for the purpose of illustration, because (1) it is widely used to represent a general load civil engineering structures may subject to; (2) its corresponding response may involve more vibration modes than harmonic excitation or free vibration. The deformation of each element and the displacement of each node are of interest in this study. Considering that it is not easy to measure the rotations at nodes in practice, rotational DOFs are eliminated in the concerned mode shapes. The strain gauges are attached to the upper face at the middle of the elements to measure the flexural deformation of the beam. As a result, 20 element strains, and 20 vertical nodal displacements are identified as the response of interest, and they are also taken as the candidate locations for strain gauges and displacements sensors. In practice, however, the sensor installment may be restricted by the approachability of each location. Meanwhile, strain gauges are supposed to be attached away from the location with stress concentration, although those locations are also hot-spots of great interest in real applications.

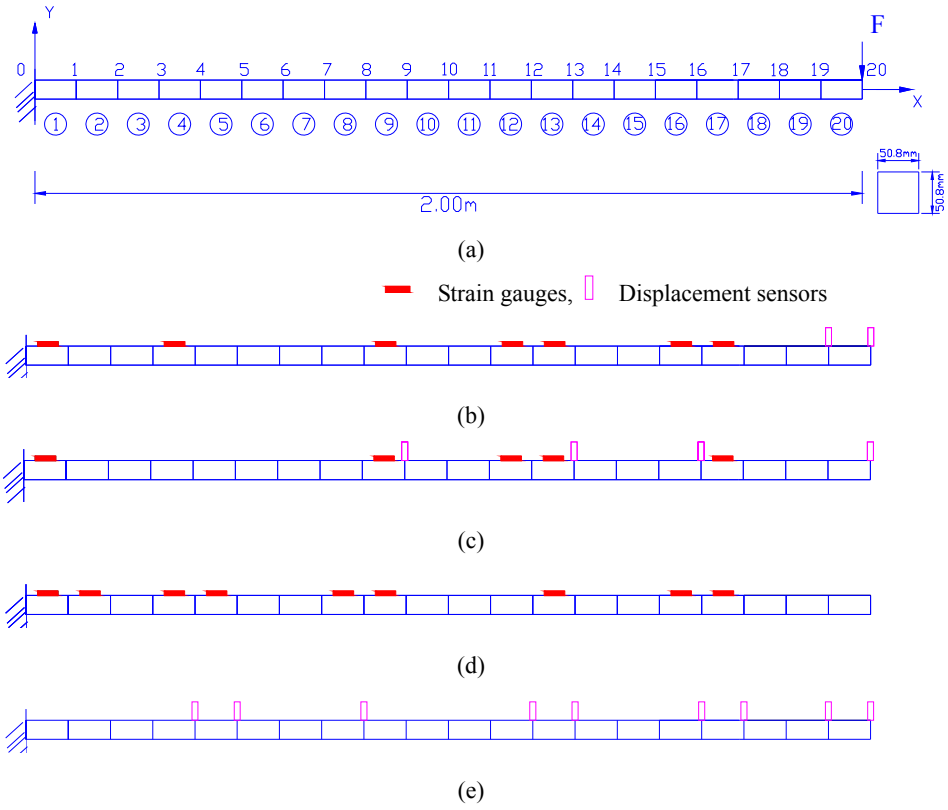

Fig. 1. Optimal sensor locations (total number of sensors = 9): (a) The finite-element model of the cantilever beam, (b) Case 1 (σ_ε =25uε,σ_d =0.7mm), (c) Case2 (σ_ε=25uε,σ_d =0.1mm), (d) Case3 (σ_ε =25uε), (e) Case4 (σ_d =0.7mm).

In this study, the noise variances are assumed to be constant for each type of sensors, and they are independent with the magnitude of response signals. In reality, sensor noise level depends not only on the type of sensors, but also on the environment and instrumentations. Hence some site-specific empirical values should be taken for sensor noise variances. The following four cases are studied and compared in the case study:

Case 1: The noise variances for strain gauges and displacement transducers are taken as σ_ε = 25με and σ_d = 0.7mm respectively.

Case 2: The noise variances for strain gauges and displacement transducers are taken as σ_ε = 25με and σ_d = 0.1mm respectively.

Case 3: Only strain gauges are installed on the beam. The noise variance for strain gauges

are taken as $\sigma_\varepsilon = 25\mu\varepsilon$.

Case 4: Only displacement transducers are installed on the beam. The noise variance for displacement transducers are taken as $\sigma_d = 0.7$mm.

The first five mode shapes are considered in the case study, and the contribution of higher modes is assumed negligible. In the first two cases, the proposed approach is adopted to optimize the locations of strain gauges and displacement transducers simultaneously, and the total number of sensors is determined based on the constraints of $\tilde{\sigma}^2_{\max} \le 1.0$ and $\tilde{\sigma}^2_{avg} \le 0.5$. In the last two cases, only one type of sensors is installed on the beam, and their performance is compared with the counterpart-Case 1. The single-type sensor systems are placed using the conventional Kammer method. The total number of sensors is set equal to that in Case 1. Fig. 1 shows the optimal sensor locations for all four cases.

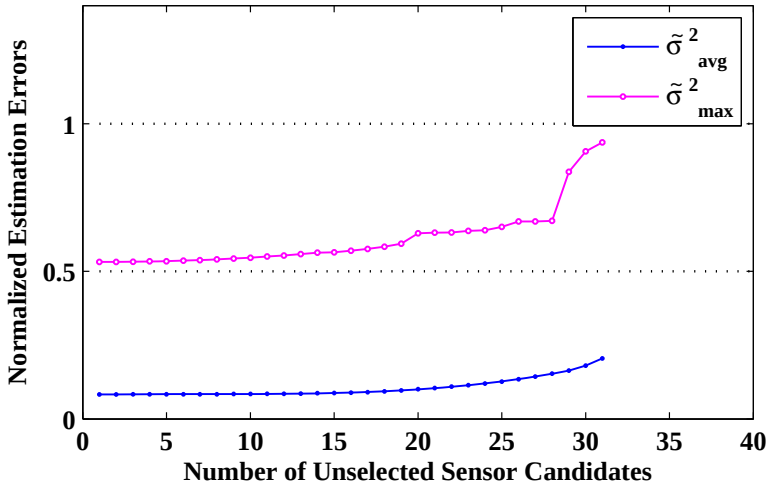

Fig. 2. Variation of theoretical estimation errors with number of sensors

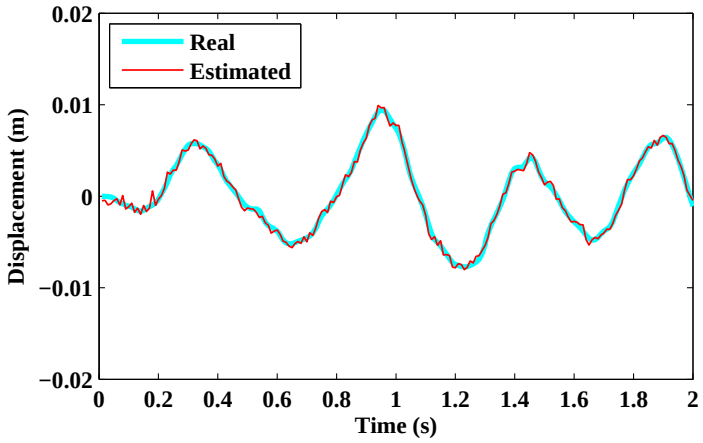

(a)

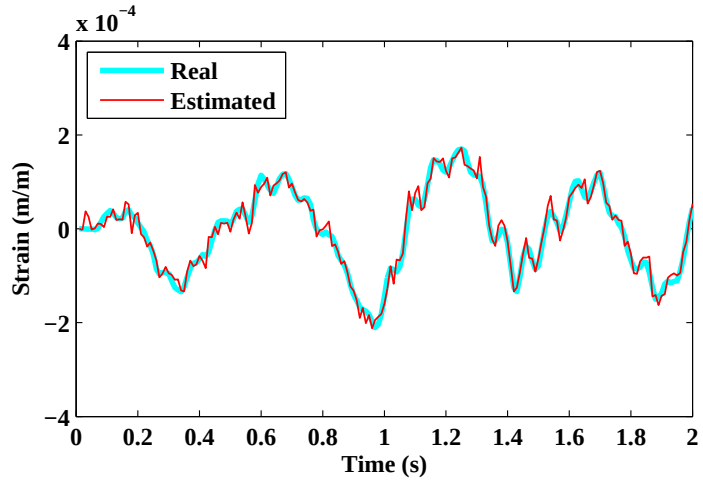

(b)

Fig. 3. Time histories of real response and estimated response (Case 1): (a) Displacement time history of Node 18, (b) Strain time history of Element 3.

In Case 1, totally 9 sensors are selected, composed of 7 strain gauges and 2 displacement transducers in y-direction, and their corresponding optimal locations are shown in Fig. 1(b). Fig.2 depicts the variation of the average and maximum normalized estimation error variance in the optimization procedure, i.e. $\tilde{\sigma}^2_{avg}$ and $\tilde{\sigma}^2_{\max}$. The sensor location which contributes most to minimize the trace of the error variance matrix $\tilde{\mathbf{\Lambda}}$ is

removed from the candidate locations in each step. Both $\tilde{\sigma}^2_{\max}$ and $\tilde{\sigma}^2_{avg}$ become larger with the decrease of the sensor number. Therefore, the final sensor number is determined when the aforementioned criteria are reached.

The responses at remaining locations are then estimated using the sensor measurements contaminated by noises. Fig. 3 illustrates the comparison of the estimated response and the real response at element 3 and node 18. As illustrated by Fig. 3, both the estimated strain and displacement can match the real response fairly well. In particular, the time histories of measurement noise and estimation error for the displacement at node 19 and the strain in element 4 are shown in Fig. 4. The comparison indicates that the estimation errors are even smaller than the measurement noise for both displacement and strain response in the simulation study. Note that the SEREP method can effectively amplify signals and attenuate noise disturbance. Fig. 5 presents the comparison between the theoretical and actual estimation errors for strains in 20 elements and vertical displacements at 20 nodes, all being normalized by sensor noise variances. Here the theoretical estimation error variances refer to the diagonal elements of error variance matrix $\tilde{\mathbf{\Lambda}}$, while the actual estimation errors are computed based on the difference between the normalized estimated response and the normalized real response. It can be seen that the theoretical values derived using the presented approach can well predict the actual errors in this case study. Slight discrepancy that can be observed is caused by truncated higher mode shapes in theoretical formulation. Since strains have more high-mode components, the discrepancy is more apparent for the strain comparison in general. It is thus necessary to cover sufficient number of mode shapes, particularly for complex structures, so that the contribution of higher modes is slight or negligible. As shown in Figs. 5(a) and (b), the values of the average and maximum normalized estimation errors are $\tilde{\sigma}^2_{avg}$=0.483 and $\tilde{\sigma}^2_{\max}$=0.915 for strains, and $\tilde{\sigma}^2_{avg}$=0.123 and $\tilde{\sigma}^2_{\max}$=0.410 for displacements. The criteria for the maximum normalized estimation error are also shown in Fig. 5 by a dashed line, and it is satisfied by actual estimated responses. Moreover, $\tilde{\sigma}^2_{\max}$ is less than 1 in both figures, which means that the estimation errors are smaller than the measurement noise levels at all the locations. In this perspective, we can conclude that it is beneficial to calculate the responses at the points even with sensor measurements. That is a major reason that the

original SEREP method is modified in this study to predict full response state instead of unmeasured response in the estimated vector. Fig. 6 illustrates the estimation errors by directly using Eq. (13), in which the non-normalized matrix $\mathbf{\Gamma}_{\mathbf{m}}$ and vector $\mathbf{y}_{\mathbf{m}}$ are used. Significant discrepancies can be observed between the theoretical values and estimated values. The issue may become more severe for large-scale complex structures. Therefore, the noise-based normalization strategy offers an effective way to improve the accuracy of estimated responses when combining strain mode shapes and displacement mode shapes together.

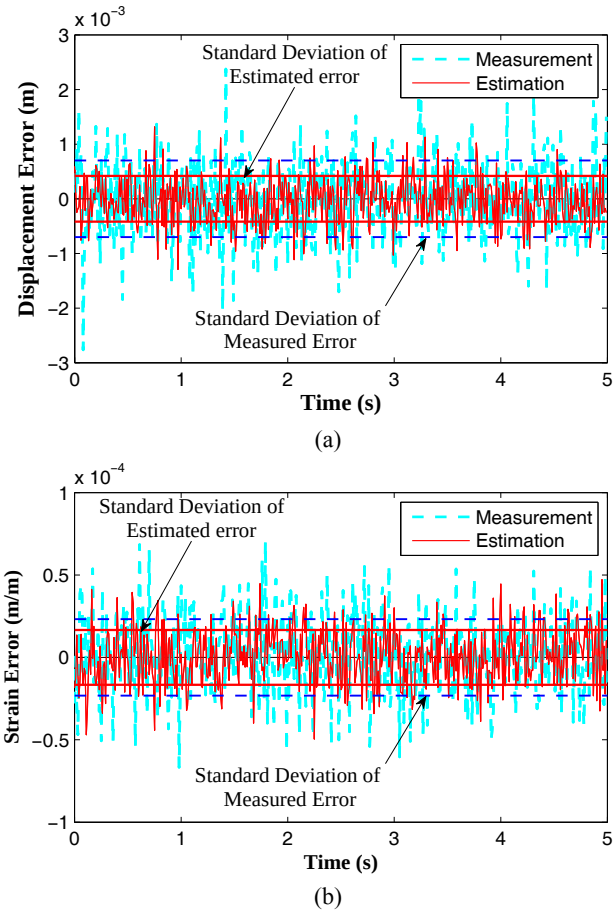

Fig. 4. Comparison of measurement noise and estimation error (Case 1): (a) Displacement error of Node 19, (b) Strain error of Element 4.

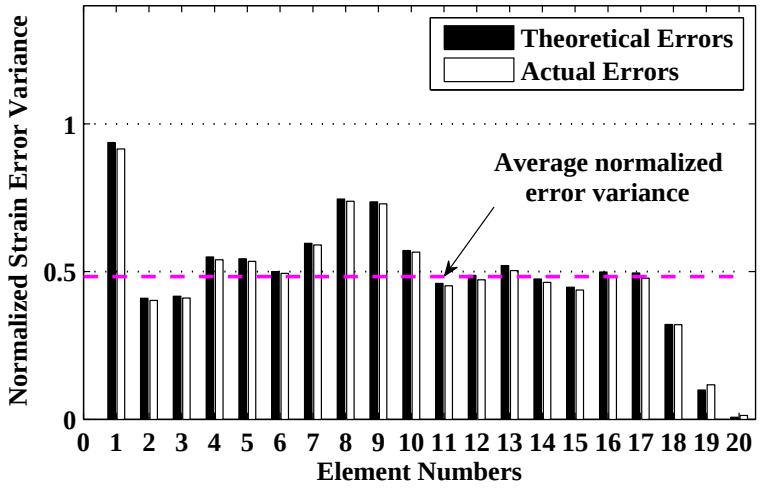

(a)

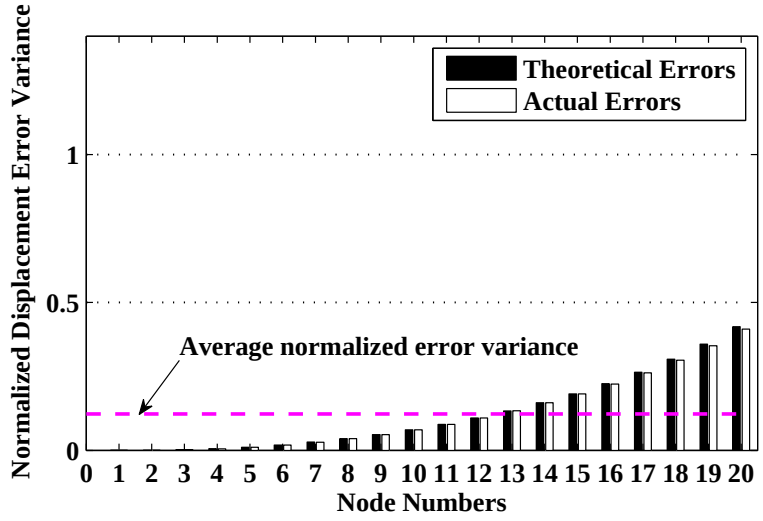

(b)

Fig. 5. Comparison of theoretical and actual estimation errors (Case 1): (a) Normalized estimation errors for strains, (b) Normalized estimation errors for displacements.

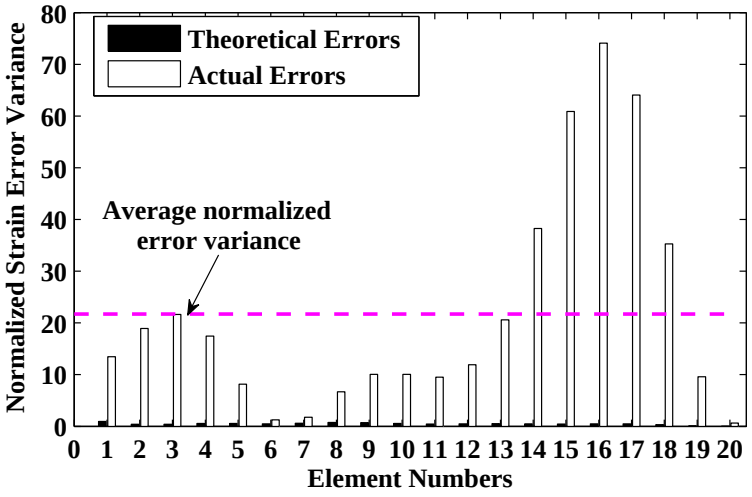

(a)

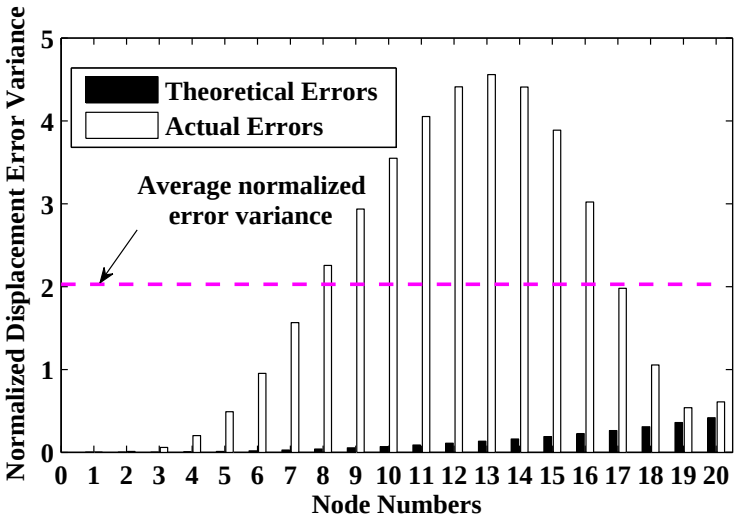

(b)

Fig. 6. Comparison of theoretical and actual estimation errors without normalization (Case 1): (a) Normalized estimation errors for strains, (b) Normalized estimation errors for displacements.

Case 2 is presented to demonstrate the effect of measurement noise upon the placement of a hybrid sensor system. The total number of sensors is 9, equal to that in Case 1. Compared with Case 1, Case 2 has the reduced displacement sensor noise variance, yet the same level of strain gauge noise. The selected sensor locations are also plotted in Fig. 1(c). Essentially the noise covariance matrix serves as a weighting matrix of mode shapes during the normalization, and hence the decrease of the displacement sensor noise actually amplifies its weighting factor relative to that for strain gauges. As a result, more displacement transducers are selected in Case 2 than in Case 1.

Cases 3 and 4 present examples of single-type sensor system, either strain gauges or displacement transducers. The noise levels are consistent with those specified in Case 1. The total numbers of sensors are 9, both equal to that in Case 1. Figs. 1(d) and (e) demonstrate the sensor locations for two cases. Figs. 7 and 9 show the distribution of normalized estimation errors for Case 3 and Case 4 respectively. In both cases, the theoretical error levels still accurately predict the actual estimation error levels. Compared with Case 1, Case 3 has similar error levels for strain estimations, ($\widetilde{\sigma}^2_{avg}$ =0.517 and $\widetilde{\sigma}^2_{\max}$ =0.718), whereas the estimation error levels for displacement response become larger ($\widetilde{\sigma}^2_{avg}$ =0.246 and $\widetilde{\sigma}^2_{\max}$ =0.973). The average normalized displacement error variance in Case 3 is about two times larger than that in Case 1 ($\widetilde{\sigma}^2_{avg}$ =0.123 and $\widetilde{\sigma}^2_{\max}$ =0.410 for displacements). Fig. 8(a) shows the time history of displacement response in Case 3 which becomes slightly worse in comparison with Case 1.

From Figs. 9 and 10, similar observations can also be made for Case 4. If only the displacement transducers are installed, the estimation errors in strain response become considerable ($\widetilde{\sigma}^2_{avg}$ =168.182 and $\widetilde{\sigma}^2_{\max}$ =346.539 for the strain responses), although the estimation of displacements is still acceptable. Such a huge discrepancy is witnessed by the strain time history in Fig. 10(b). It is because that the displacement responses generally contain less high-frequency components than strain responses. Through the comparison of Cases 1, 3 and 4, it is seen that the optimized hybrid sensor system, a combination of displacement transducers and strain gauges, contains more information of the entire structural response than single-type sensor system, provided that the data from multi-type

sensors can be appropriately fused.

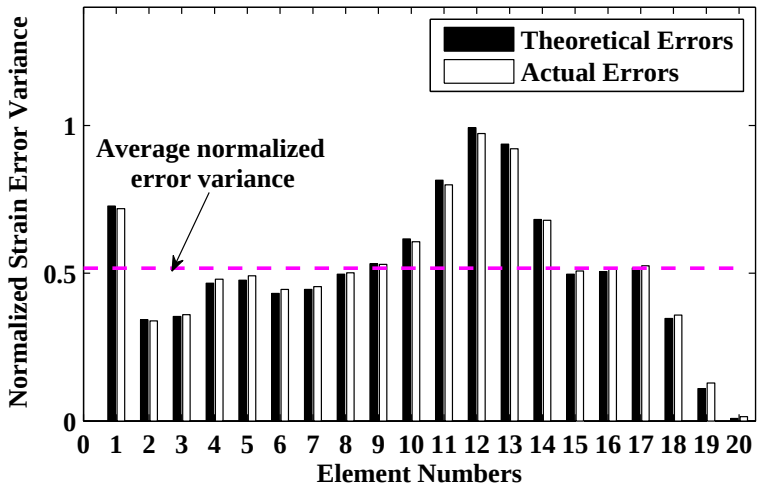

(a)

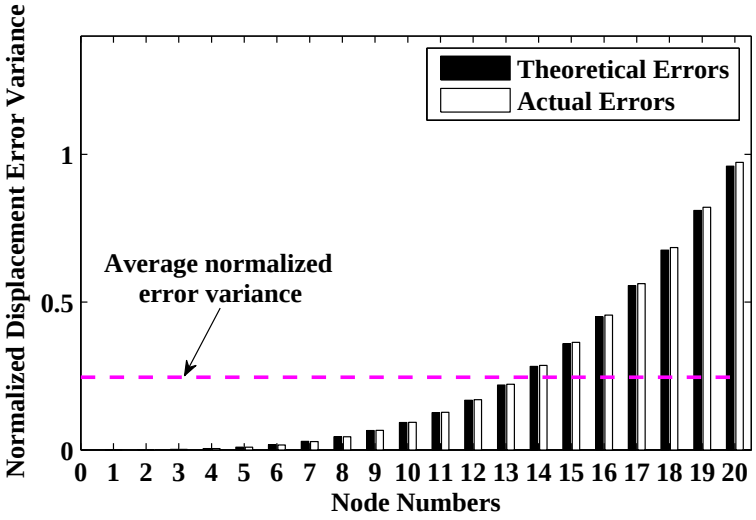

(b)

Fig. 7. Comparison of theoretical and actual estimation errors (Case 3): (a) Normalized estimation errors for strains, (b) Normalized estimation errors for displacements.

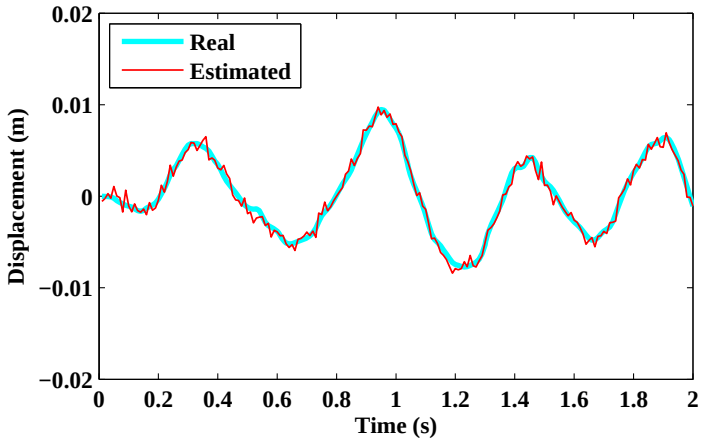

(a)

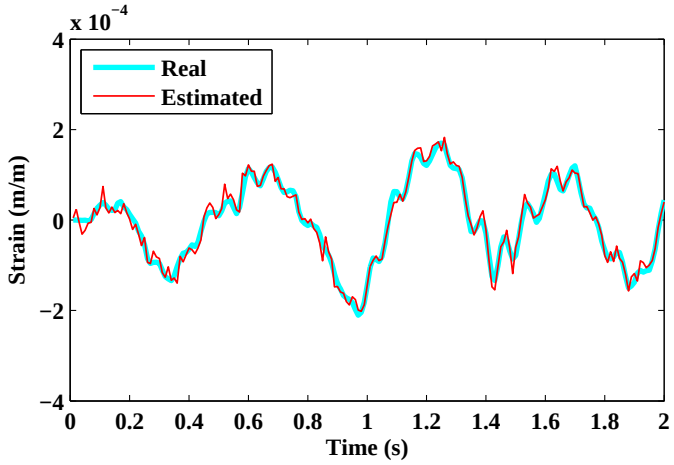

(b)

Fig. 8. Time histories of real response and estimated response (Case 3): (a) Displacement time history of Node 18, (b) Strain time history of Element 3.

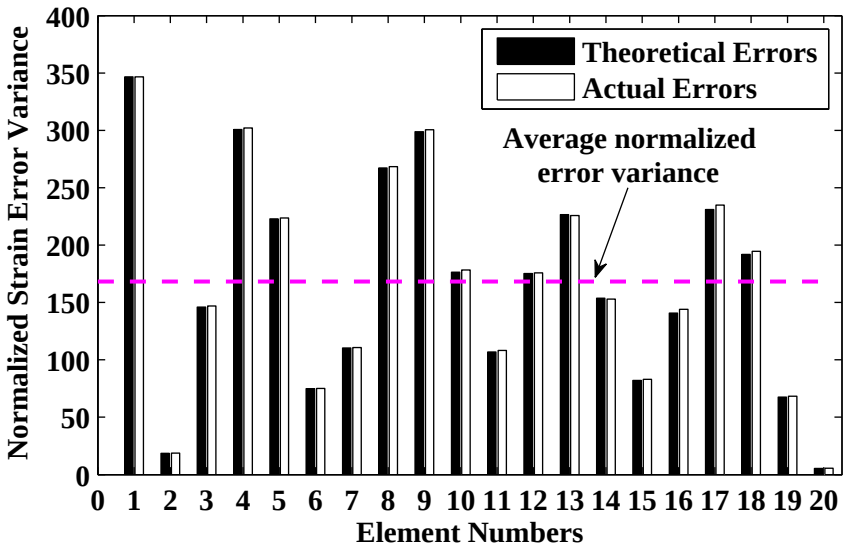

(a)

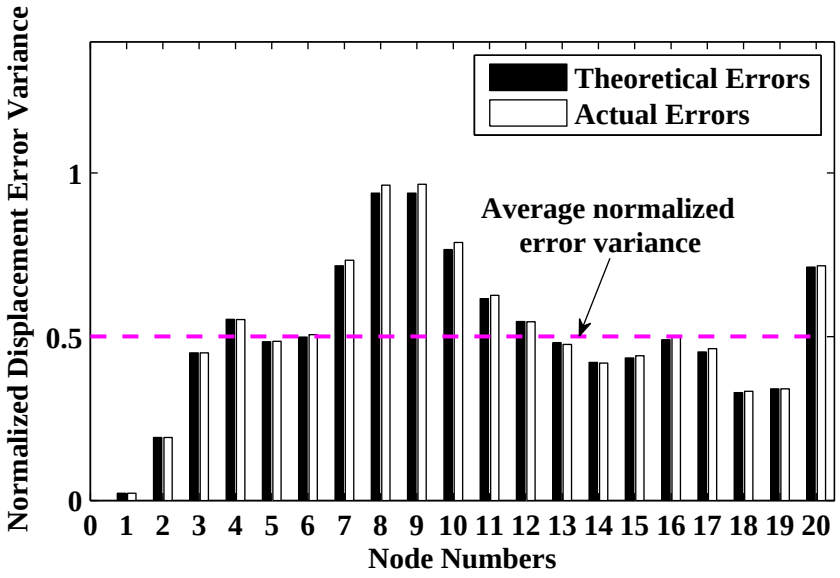

(b)

Fig. 9. Comparison of theoretical and actual estimation errors (Case 4): (a) Normalized estimation errors for strains, (b) Normalized estimation errors for displacements.

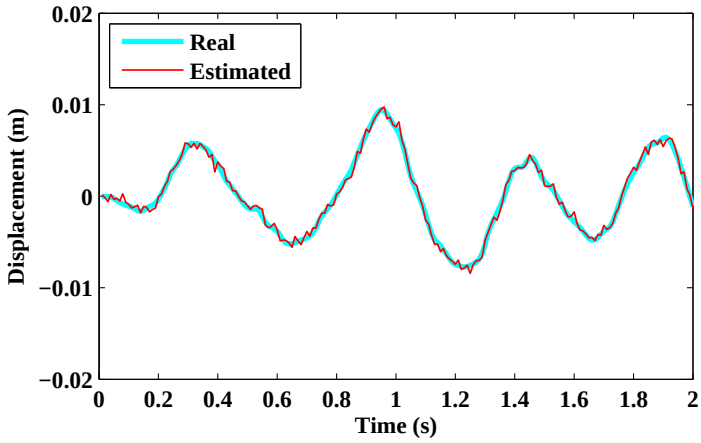

(a)

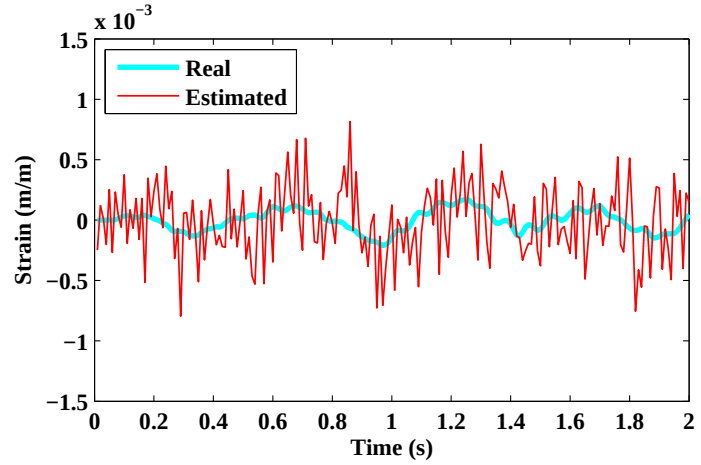

(b)

Fig. 10. Time histories of real response and estimated response (Case 4): (a) Displacement time history of Node 18, (b) Strain time history of Element 3.

5. Conclusions

An optimal sensor placement approach is presented in this study for monitoring systems with both strain gauges and displacement transducers. Instead of being carried out in two separate courses, the placement of two types of sensors is optimized simultaneously in this approach. Subsequently, the measurements from both types of sensors are employed collectively to estimate the response of the entire structure. The optimization objective is to

best estimate structural strains and displacements of interest using limited measurements from sensors, and the total number of sensors is determined to achieve the desired error levels in structural response estimations. Noise-normalized responses and mode shapes are used in this approach. A numerical analysis of a cantilever beam indicates that this approach offers an effective way to design such a hybrid sensor system as a whole and reduce a relatively large initial candidate location set to a much smaller optimum set. The actual estimation error levels induced by measurement noises can be fairly well quantified by the theoretical formulation, and the target estimation error levels can be successfully achieved through the optimization procedure in numerical study. The results of a comparative study also demonstrate that the hybrid sensor network with multiple types of sensors can provide more complete and accurate information about structural response, compared with single-type sensor systems. It should be pointed out that in practice the estimation accuracy may be affected by numerous factors such as the uncertainty in measurement noise, the influence of higher modes, the discrepancy between FEM and structures, and non-synchronization of strain and displacement signals, etc. Therefore an actual estimation error is expected be larger than the theoretical prediction. An experimental verification needs to be carried out in future study to assess the effect of these factors.

Acknowledgment

The authors are grateful for the financial support from The Hong Kong Polytechnic University through a Niche Areas Funding (Poly1-BB68).

Reference

1. Q.G. Fei, Y.L. Xu, C.L. Ng, K.Y. Wong, W.Y. Chan and K.L. Man, Structural health monitoring oriented finite element model of Tsing Ma Bridge tower, *International Journal of Structural Stability and Dynamics*, 7(4) (2007) 647-668.

2. B. Zhu, A.Y.T. Leung, C.K. Wong and W.Z. Lu, On-line health monitoring and damage detection of structures based on the wavelet transform, *International Journal of Structural Stability and Dynamics,* 8(3) (2008) 367-387.

3. P.C. Shah and F.E. Udwadia, A methodology for optimal sensor locations for identification of dynamic system, *Journal of Applied Mechanics-Transactions of the Asme*, 45(1) (1978) 188-196.

4. D.C. Kammer, Sensor placement for on-orbit modal identification and correlation of

large space structures, *Journal of Guidance, Control and Dynamics*, 14(2) (1991) 251-259.
5. D.C. Kammer, Effect of noise on sensor placement for on-orbit modal identification of large space structures, *Journal of Dynamic Systems, Measurement, and Control*, 114 (1992): 436-443.
6. D.C. Kammer, Enhancement of on-orbit modal identification of large space structures through sensor placement. *Journal of Sound and Vibration*, 171(1) (1994) 119-139.
7. D.C. Kammer and R.D. Brillhart, Optimal sensor placement for modal identification using system-realization methods, *Journal of Guidance, Control and Dynamics*, 19(1996) 729–731.
8. D. C. Kammer and M.L. Tinker, Optimal placement of triaxial accelerometers for modal vibration tests, *Journal of Mechanical Systems and Signal Processing*, 18(1) (2004) 29–41.
9. F.E. Unwadia, Methodology for optimal sensor locations for parameter identification in dynamic system, *Journal of Engineering Mechanics*, 120 (1994) 368-390.
10. P. H. Kirkegaard and R. Brincker, On the optimal locations of sensors for parametric identification of linear structural systems, *Journal of Mechanical Systems and Signal Processing*, 8(6) (1994) 639–647.
11. J.E. T. Penny, M.I. Friswell and S. D. Garvey, Automatic choice of measurement location for dynamic testing, *AIAA Journal*. 32 (1994) 407–414.
12. R.G Cobb, and B.S Liebst, Sensor placement and structural damage identification from minimal sensor information, *AIAA Journal*, 35(2) (1997) 369-374.
13. N. Imamovic, Model validation of large finite element model using test data, PhD Thesis, Imperial college London, 1998.
14. Z.Y. Shi, S.S. Law and L.M. Zhang, Optimum sensor placement for structure damage detection, *Journal of Engineering Mechanics*, 126(11) (2000) 1173-1179.
15. M. Meo and G. Zumpano, On the Optimal Sensor Placement Techniques for a Bridge Structure. *Engineering Structures,* 27 (2005) 1488 – 1497.
16. C. Papadimitriou, J.L. Beck and S.K. Au, Entropy-based optimal sensor location for structural model updating, *Journal of Vibration and Control,* 6 (2000)781-800.
17. C. Papadimitriou, Optimal sensor placement for parametric identification of structural systems, *Journal of Sound and Vibration*, 278(4-5) (2004) 923–947.
18. C. Papadimitriou, Pareto optimal sensor locations for structural identification, *Computer Methods in Applied. Mechanics and Engineering*, 194(12-16) (2005) 1655–1673.
19. K.V. Yuen, L.S. Katafygiotis, C. Papadimitriou and N.C. Mickleborough, Optimal sensor placement methodology for identification with unmeasured excitation, *Journal of*

Dynamic Systems, Measurement and Control 123(4) (2001) 677–686.
20. F.M. Hemez and C. Farhat, An energy based optimum sensor placement criterion and its application to structure damage detection, *Proceedings of the 12th International Conference. on Modal Analysis*, Society of Experimental Mechanics, Honolulu ,1994, pp.1568–1575.
21. M. Salama, T. Rose and J. Garba, Optimal Placement of Excitations and Sensors for Verification of Large Dynamical Systems, *Proceedings of the 28th Structures, Structural Dynamics, and Materials Conference*, Monterey, CA ,1987,pp.1024-1031.
22. Y.T. Chung and J.D. Moore, On-orbit sensor placement and system identification of space station with limited instrumentations, *Proceedings of the 11th International Modal Analysis Conference*, Kissimmee, FL,1993,pp.41-46.
23. G. Heo, M.L.Wang and D. Satpathi, Optimal transducer placement for health monitoring of long span bridge. *Soil Dynamics and Earthquake Engineering,* 16 (1997) 495–502.
24. D.S. Li, H.N. Li, and C.P. Fritzen, The connection between effective independence and modal kinetic energy methods for sensor placement, *Journal of Sound and Vibration*, 305(4-5) (2007) 945-955.
25. B. Jarvis, Enhancements to modal testing using finite elements, *Journal of Sound and Vibration*, 25(8) (1991) 28-30.
26. P.Tongpadungrod, T.D.L. Rhys and P.N. Brett, An approach to optimise the critical sensor locations in one-dimensional novel distributive tactile surface to maximize performance, *Sensors & Actuator*s A, 105 (2003) 47–54.
27. K.B.Lim, Method for optimal actuator and sensor placement for large flexible structures, *Journal of Guidance, Control and Dynamics,* 15 (1992) 49–57.
28. T.G. Carne and C.R. Dohrmann, A modal test design strategy for model correlation, *Proceedings of the 13th International Modal Analysis Conference*, Nashville, TN,1995.
29. J.M. Beal, A. Shukla, O.A. Brezhneva, and M.A. Abramson, Optimal sensor placement for enhancing sensitivity to change in stiffness for structural health monitoring, *Optimization and Engineering*, 9(2) (2008) 119-142.
30. L. Yao, W.A. Sethares, and D.C. Kammer, Sensor placement for on-orbit modal identification via a genetic algorithm, *AIAA Journal*, 31(10) (1993) 1922-1928.
31. K. Worden, A.P. Burrows, and G.R. Tomlinson, A combined neural and genetic approach to sensor placement, *Proceedings of the 13th International Modal Analysis Conference*, Nashville, TN, 1995, pp.1727-1736.
32. W.M. Said, and W.J. Staszewski, Optimal sensor location for damage detection using

mutual information, *11th International Conference on Adaptive Structures and Technologies*, Nagoya, 2000, pp.428-435.
33. K.Worden and A. P. Burrows, Optimal sensor placement for fault detection, *Engineering Structures,* 23 (2001) 885-901.
34. H.Y. Guo, L. Zhang, L.L. Zhang and J.X. Zhou, Optimal placement of sensors for structural health monitoring using improved genetic algorithms. *Smart Materials and Structure*, 13(3) (2004) 528-534.
35. W. Liu, W.C. Gao, Y. Sun, M.J. Xu, Optimal sensor placement for spatial lattice structure based on genetic algorithms, *Journal of Sound and Vibration*, 317(1-2) (2008) 175-189.
36. A.R.M. Rao and G. Anandakumar, Optimal placement of sensors for structural system identification and health monitoring using a hybrid swarm intelligence technique. *Smart Materials and Structures*, 16 (2007) 2658-2672.
37. R.J. Barthorpe and K. Worden, Sensor placement optimization, *Encyclopedia of Structural Health Monitoring*, John Wiley & Sons,Ltd, 2009.
38. N.S.Ottosen and H. Petersson, Introduction to the Finite Element Method, Prentice Hall, Europe, 1992.
39. D.J. Ewins, Modal testing: theory, practice and application. 2nd ed. Research Studies Press LTD, Letchworth, England, 2000.
40. J.C. O'Callahan, P. Avitabile and R. Riemer, System equivalent reduction expansion process, *Proceedings of the Seventh International Conference on Modal Analysis*, Las Vegas, Nevada, February 1989.
41. F.E. Unwadia and J.A. Garba, Optimal sensor locations for structural identification. *Proceeding of the Workshop on Identification and Control of Flexible Space Structures*,1985, pp.247-261.